Applied Physics Letters

RESEARCH ARTICLE | APRIL 21 2023

Miniaturized microsphere-assisted microscopy

Stephane Perrin ✉; Robin Pierron; Philippe Gerard; ... et. al

Check for updates

Appl. Phys. Lett. 122, 161108 (2023)
https://doi.org/10.1063/5.0135346

CrossMark

View Online

Export Citation

Articles You May Be Interested In

The 3D heat flux density distribution on a novel parabolic trough wavy absorber

AIP Conference Proceedings (May 2016)

A 1D thermal model for PTR including pressure drop and kinetic energy change within the fluid: Conventional absorber tube vs. S-curved

AIP Conference Proceedings (July 2019)

A century of superconducting technology

AIP Conference Proceedings (June 2012)

AIP Publishing

Downloaded from http://pubs.aip.org/aip/apl/article-pdf/doi/10.1063/5.0135346/16951738/161108_1_5.0135346.pdf

Applied Physics Letters ARTICLE scitation.org/journal/apl

Miniaturized microsphere-assisted microscopy

Cite as: Appl. Phys. Lett. **122**, 161108 (2023); doi: 10.1063/5.0135346
Submitted: 18 November 2022 · Accepted: 9 April 2023 ·
Published Online: 21 April 2023

View Online Export Citation CrossMark

Stephane Perrin,[1,a)] Robin Pierron,[1] Philippe Gerard,[1,2] Paul Montgomery,[1] and Sylvain Lecler[1,2]

AFFILIATIONS

[1]ICube Research Institute, University of Strasbourg – CNRS, 300 Boulevard Sébastien Brant, 67412 Illkirch, France
[2]INSA Strasbourg, 24 Boulevard de la Victoire, Strasbourg, France

[a)]**Present address:** Photonics Bretagne, 22300 Lannion, France. **Author to whom correspondence should be addressed:** sylvain.lecler@insa-strasbourg.fr

ABSTRACT

Microsphere-assisted microscopy is a sub-diffraction-limited imaging technique, which uses dielectric microspheres to collect the near-field information of an object. In this work, the bulk of the classical microsphere-based system is reduced by the simple introduction of a ball lens. The miniaturized imaging system has been designed and vertically assembled. Performance of the proposed dual-sphere system is quantified through numerical simulations and experiments. A theoretical impulse response with a full width at half maximum smaller than half of the wavelength is reached in air. As a proof of concept, 500-nm-period standard gratings and gold nanoparticles are observed without a classical objective, validating a sub-wavelength resolution with a high imaging quality and low aberrations over the field of view.

Published under an exclusive license by AIP Publishing. https://doi.org/10.1063/5.0135346

Stretching the limits due to the diffraction of light so as to be able to visualize feature sizes smaller than $\lambda/2$ (λ, the wavelength of light) has received much interest in optical microscopy. This has led to several approaches that have succeeded in breaking the diffraction limit up to a value of $\lambda/30$. Among them, near-field scanning optical microscopy has made it possible to characterize nano-structures with a high efficiency.[1] Within this range of resolutions, stimulated-emission-depletion microscopy[2] and photo-activated localization microscopy[3] are also able to explore infinitely small biological elements. These two super-resolved fluorescence techniques were brought to the forefront in 2014 with the Nobel Prize for Chemistry.[4] Nonetheless, lateral scanning, complex alignment of the optical components, or photo-toxic illumination of the sample is required to reach super resolution. In addition, label-free imaging techniques providing sub-diffraction-limit resolution (i.e., a resolution up to $\lambda/6$) have been developed among which structured illumination microscopy,[5] solid immersion lenses,[6] and metamaterial-based components.[7,8]

Another technique consists of imaging through dielectric microspheres, which has been demonstrated in air[9] and in immersion.[10] Introducing a dielectric microsphere in front of a white-light microscope allows the lateral resolution of the microscope to be considerably increased. Microspheres are assumed to act as a *superlens* through which the high spatial frequencies of the object are converted into propagating modes.[11] Investigations have made it possible to not only define the physical phenomenon behind the sub-diffraction-limit resolution[12–14] but also to quantify the effects of the coherence of light on the imaging quality[15] and to determine the influence of the geometrical and the optical parameters on the imaging formation.[16,17] As well as the lateral resolution reaching up to $\lambda/5$ in air, full-field microsphere-assisted microscopy is easier to implement and more efficient than other sub-diffraction-limit imaging techniques.[18] Microsphere-based systems have, thus, been demonstrated to be useful in biological imaging[19–22] and for the topography reconstruction of transparent nanodots with a high spatial accuracy.[23]

In microsphere-assisted microscopy, a magnified image of the high-spatial-frequency details of the object is generated[24] below or above the object plane depending on various parameters.[25] Then, a microscope objective usually collects and directs this image onto a camera. Two-microbeads-based systems have more recently been developed to increase the imaging contrast[26] or to enhance the lateral magnification[27,28] in microsphere-assisted microscopy. In the experiments presented, due to the significant difference in size between the microscope objective and the microsphere, manipulating and positioning the microspheres above the object area to be observed is not simple despite suggested advances.[29–31] Furthermore, the arrangement of the optical system remains bulky.

In this work, the classical objective is substituted for a ball lens in order to miniaturize the optical head and still achieve high lateral resolution. The compact dual-sphere system consists of two glass spheres and a two-dimensional detector. The design aspects of the dual-sphere optical system have been studied using both electromagnetic simulation and ray-tracing analysis in order to optimize the performance.

Downloaded from http://pubs.aip.org/aip/apl/article-pdf/doi/10.1063/5.0135346/16951738/161108_1_5.0135346.pdf

Published under an exclusive license by AIP Publishing

The system has been experimentally assembled to demonstrate the imaging feasibility through direct experimental measurements.

The design of the proposed dual sphere system is illustrated in Fig. 1(a). The microsphere has a diameter D_{ms} of 42 μm and a refractive index n_{ms} of 1.52 in the visible range. Deposited on the sample, the microsphere generates an intermediate magnified image (containing the near-field information of the object). The ball lens then collects the intermediate image from the microsphere to form a final real image on the camera. The ball lens has a diameter D_{bl} and a refractive index n_{bl} of 300 μm and 1.52, respectively. In the experiment, a glass layer (i.e., the protection windows of the camera) is between the ball lens and the camera plane, in contact with the last surface of the ball lens. The optical path length of the protection glass is of 320 μm and the distance between the camera plane and the last surface is 620 μm. These values were measured using an interference-based profiler.

To demonstrate its sub-diffraction-resolution ability, the microsphere alone was first numerically simulated using a 2D finite element method (COMSOL Multiphysics®). The polarization is transverse electric (TE), being an electric field orthogonal to the simulation plane. The maximum element size of the mesh is of $\lambda/10$ (with $\lambda = 550$ nm). The object consists of two symmetric point sources A and B in air

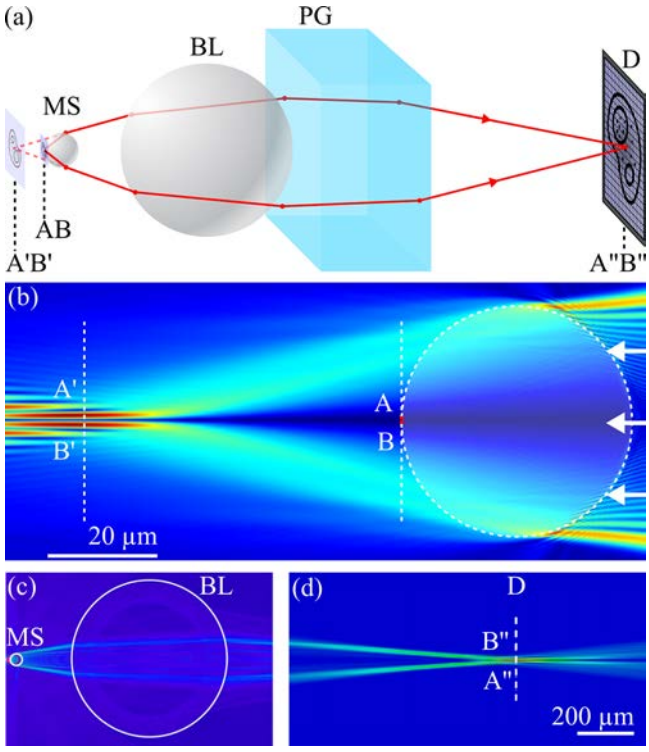

FIG. 1. (a) Layout of the dual-sphere-based imaging system. MS, microsphere; BL, ball lens; PG, protection glass; and D, detector. (b) Normalized modulus of the time-reversal electric field in air. The planes of the object $\overline{AB}$ and of the intermediate virtual image $\overline{A'B'}$, as well as the microsphere, are drawn with a white-dashed line only for showing their position. $\lambda = 550$ nm, $D_{ms} = 42$ μm, and $n_{ms} = 1.52$. (c) Normalized modulus of the electric field through the dual-sphere imaging system. $D_{bl} = 300$ μm and $n_{bl} = 1.52$. (d) Normalized squared modulus of the electric field emanating from the dual-sphere imaging system. An image $\overline{A''B''}$ of the object $\overline{AB}$ is formed in the conjugated image plane.

having an opposite initial phasor.[15] Due to the low optical path differences compared to the coherence length of the source (a few tens of micrometers), the phase difference between two close objects of the sample cannot be neglected.[32] The behavior in electromagnetic simulation is more complex than in a classical incoherent imaging processes. Indeed, interferences may occur between the two point sources. And, if their relative phase difference is smaller than π rad, the image contrast of the two points would be lower. The transverse distance $\overline{AB}$ between the two point sources is of 300 nm (i.e., $\lambda/1.8$). Hence, the microsphere generates two virtual intermediate images A' and B'. To visualize them, a time-reversal propagation is achieved in free space [Fig. 1(b)] where the two maxima correspond to the two virtual images.[17] The virtual image plane is at an axial distance of 84 μm from the center of the microsphere. Moreover, the transverse magnification factor of the microsphere alone is of $\times 2.67$. This latter has been averaged by varying the distance $\overline{AB}$. Finally, the image numerical aperture (i.e., the angle of the beam exiting the microsphere) is of 0.16 and the field of view is of around 6 μm.

The complete dual-sphere system has then been simulated by first propagating light through the two spheres [Fig. 1(c)] with the 2D TE finite element method (maximum element size $= \lambda/10$). Second, the waves are propagated in free space from the center of the protection window to the camera plane using the radiation spectrum method [Fig. 1(d)]. The latter method, through a permanent harmonic field hypothesis, has the advantage of having a fast calculation time.[33] The axial increment is of 0.3 μm. The two maxima A'' and B'' correspond to two real images on the sensor chip of the camera. According to the simulation, the magnification factor $\overline{A''B''}/\overline{AB}$ of the dual-sphere system is of $\times 9.2$. Assuming the imaging system to be linear, the ball lens magnification is, thus, of $\times 3.5$. In the image plane, the impulse response has been calculated by simulating only one point source. Its full width at half maximum (FWHM) is of around 1.6 μm. In the object plane, this leads to a FWHM of 175 nm, corresponding to $\lambda/3.2$.

The ability of the ball lens to resolve the features in the intermediate virtual plane depends not only on the magnification from the microsphere but also on the image numerical aperture of the microsphere. With an entrance numerical aperture of 0.16, the ball lens would not be able to resolve features smaller than 1.7 μm in the intermediate image plane, being of around 640 nm in the object plane. This latter appears to be lower than the one numerically determined (i.e., FWHM = 175 nm). Actually, the cone of light could, thus, be higher than 0.16 which was previously estimated only using the high-intensity beams exiting the microsphere. Indeed, the beams having a lower intensity have not been considered despite they contain high-spatial-frequency information. This hypothesis could also explain the gallery modes propagating at the periphery within the ball lens [Fig. 1(c)] as well as performance further experimentally demonstrated.

Ray tracing analysis (Zemax OpticStudio) of the system was also implemented (Fig. 2). Despite the fact that ray-tracing may not be most appropriated for simulating the microsphere, it, nonetheless, makes it possible to qualify the optical aberrations of the ball lens and, further, to optimize the performance. As expected, the combination of a microsphere with a ball lens leads to spherical aberrations, influencing the evolution of the imaging contrast [Fig. 2(d)]. The spherical aberration factor (Coddington shape factor) of the microsphere alone is of around -1.2.[34] However, by adjusting the distance between the last microsphere surface and the ball lens surface at around 31 μm, the

Downloaded from http://pubs.aip.org/aip/apl/article-pdf/doi/10.1063/5.0135346/16951738/161108_1_5.0135346.pdf

Published under an exclusive license by AIP Publishing

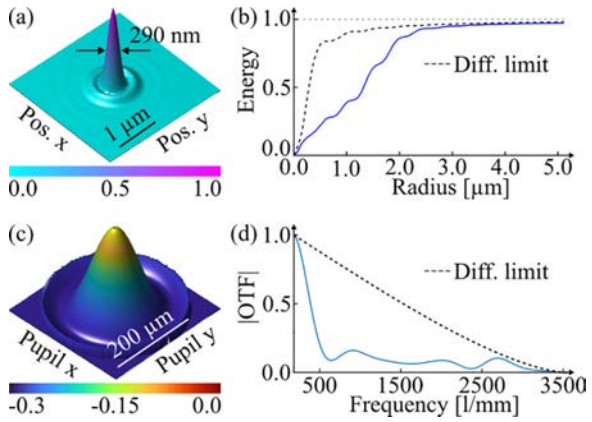

FIG. 2. Ray-tracing analysis of the dual-sphere imaging system. $\lambda = 550$ nm. (a) Normalized point spread function distribution. (b) Fraction of the encircled energy as a function of the radial distance. (c) Wavefront distribution (in λ) over unit pupil function. (d) Normalized modulation transfer function as a function of the spatial frequency. OTF: Optical transfer function. In (b) and (d), the dashed lines represent the evolution curves of a diffraction-limited system.

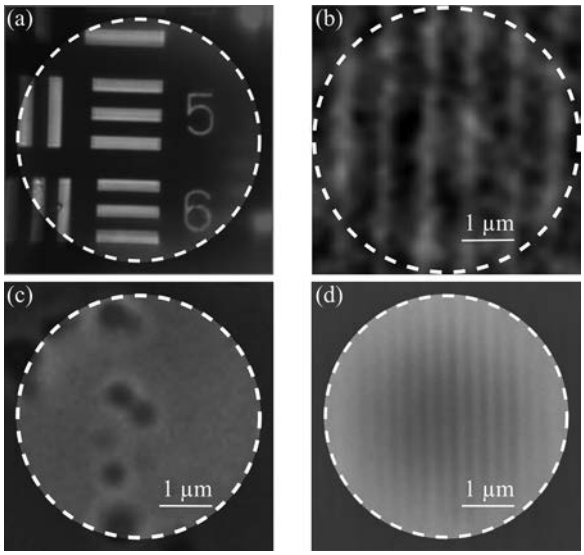

FIG. 3. Experimental measurements through the dual-sphere imaging system. (a) See-through ball lens image of a 1951 USAF target, (b) 400-nm-groove Ronchi grating, (c) 500-nm-diameter gold nanoparticles, and (d) 250-nm-linewidth transparent grating.

global optical aberrations have been reduced: the peak to valley and the root mean square of the wavefront in the image plane are now of 0.30λ and 0.07λ, respectively. Moreover, the magnitudes of the defocus (Z_4) and the oblique trefoil (Z_9) along the optical axis are of -0.09λ and 0.11λ, respectively. The FWHM of the point spread function is of around 290 nm, being higher than using COMSOL Multiphysics®. Indeed, the evanescence-wave collection by the microsphere and the coherence effects due to the low optical path differences are not considered. Thus, in ray-tracing, the calculated FWHM can only be higher than half of the wavelength (i.e., 275 nm).

Based on this optimized design, a dual-sphere imaging system was built in the transmission mode. A LED light source with an illumination peak at 550 nm illuminates the sample. A soda-lime-glass microsphere and an N-BK7 ball lens form the image of the sample on the camera (Basler, acA3800–14um). To build the system, the camera points upwards and the ball lens sits on the camera protection glass. The microsphere remains naturally attached to the object surface due to electrostatic forces. The protection glass of the camera was in the good range. The image adjustment has been made using the distance between the two spheres. This explains the small difference between experiment and simulation. First, the ball lens alone is used to image the sample. Then a microsphere is searched and placed in the center (moving the sample). Finally, the virtual image achieved by the microsphere is searched moving up the sample. Measurements show that the ball lens alone provides a lateral magnification of $\times 3.9$ [Fig. 3(a)], in agreement with the numerical estimation. And, the magnification of the dual sphere system was estimated using an 800-nm-period Ronchi grating [Fig. 3(b)] to be equal to $\times 8.85$. The impulse response is sampled over 2 pixels. The measurement of the Ronchi grating shows distortions of the vertical lines, revealing the influence of the microsphere quality. In the center of the field of view, a bright spot also occurs due to the illumination condition. Randomly deposited gold nanoparticles and a 250-nm-linewidth (500 nm period) transparent grating (with a refractive index of 1.7) were then observed through a high-quality microsphere. In this experiment, the dual-sphere system performs high quality imaging, so demonstrating its ability to resolve small features. In Fig. 3(d), the contrast has been numerically increased in order to highlight the transparent grooves. The use of dark-field illumination could also increase the contrast.[22]

This proof of concept has demonstrated the imaging ability of a high-resolution dual-sphere system which could be exploited, for example, in microfluidics to improve the detection sensitivity.[35] Further improvements of the system can also be considered to reach super-resolution. First, in the numerical analysis [Fig. 1(c)], the distance between the cover glass and the image plane is higher than the real distance between the protection glass and the camera chip (620 μm), a detail that could be optimized. In the experiment, the ball lens is positioned so as to obtain an in-focus image. Also, the sampling of the impulse response is close to the theoretical Nyquist criterion, whereas it should be a factor of two in order to avoid undersampling. This could be achieved by either using a camera with smaller pixels or using a smaller microsphere to increase the resolving power of the dual-sphere system.[14] To compensate the reduction in the lateral field of view through the use of a small microsphere, a matrix arrangement of microspheres could be considered.[36] In addition, the microsphere should be raised for biological imaging in order to perform contactless measurements.[30] For this purpose, the optical components could be vertically assembled and integrated not only to be axially positioned above the sample but also to be batch fabricated, leading to a compact imaging system of around 1 mm in size.[37] Finally, a low-optical-aberration design could also be investigated.[38]

The proof of concept of the miniaturization of a microsphere-assisted microscope is demonstrated in air by means of numerical analysis and experimental measurements. For this purpose, a ball lens replaces the classical microscope objective to collect the magnified image generated by a microsphere. The dual-sphere system with smaller pixels could theoretically resolve features having a size of

Downloaded from http://pubs.aip.org/aip/apl/article-pdf/doi/10.1063/5.0135346/16951738/161108_1_5.0135346.pdf

Published under an exclusive license by AIP Publishing

175 nm (λ/3.2). Gold nanoparticles and 250-nm-groove transparent grating have been observed with high imaging quality. Future enhancements could be considered to improve the performance of the system so as to be suitable for use in biological and microfluidic applications for examples.

This work was funded by the SATT Conectus Alsace (SIBiC project) and FRCR—Grand Est (MIRAGE project). We would like to thank Amir Nahas for providing gold nanoparticles and Jesse Schiffler for measuring the protection glass thickness of the camera using a Zygo optical profiler. Also, the authors thank Amandine Elchinger for revising the manuscript content.

AUTHOR DECLARATIONS

Conflict of Interest

The authors have no conflicts to disclose.

Author Contributions

Stephane Perrin: Conceptualization (equal); Data curation (equal); Formal analysis (equal); Funding acquisition (equal); Investigation (equal); Methodology (equal); Project administration (equal); Resources (equal); Software (equal); Supervision (equal); Validation (equal); Visualization (equal); Writing – original draft (equal); Writing – review & editing (equal). **Robin Pierron:** Conceptualization (equal); Formal analysis (equal); Methodology (equal); Visualization (equal). **Philippe Gerard:** Data curation (equal); Investigation (equal); Software (equal); Visualization (equal); Writing – review & editing (equal). **Paul Montgomery:** Project administration (equal); Supervision (equal); Validation (equal); Writing – review & editing (equal). **Sylvain Lecler:** Conceptualization (equal); Investigation (equal); Methodology (equal); Project administration (lead); Supervision (lead); Validation (equal); Visualization (equal); Writing – review & editing (equal).

DATA AVAILABILITY

The data that support the findings of this study are available within the article.

REFERENCES

[1]D. Pohl, W. Denk, and M. Lanz, "Optical stethoscopy: Image recording with resolution λ/20," Appl. Phys. Lett. **44**, 651–653 (1984).
[2]S. W. Hell, "Far-field optical nanoscopy," Science **316**, 1153–1158 (2007).
[3]E. Betzig, G. H. Patterson, R. Sougrat, O. W. Lindwasser, S. Olenych, J. S. Bonifacino, M. W. Davidson, J. Lippincott-Schwartz, and H. F. Hess, "Imaging intracellular fluorescent proteins at nanometer resolution," Science **313**, 1642–1645 (2006).
[4]See https://www.nobelprize.org/prizes/chemistry/2014/summary/ for NobelPrize.org, "The Nobel Prize in Chemistry 2014," (2018) (accessed 11 April 2023).
[5]M. G. L. Gustafsson, "Surpassing the lateral resolution limit by a factor of two using structured illumination microscopy," J. Microsc. **198**, 82–87 (2000).
[6]S. M. Mansfield and G. S. Kino, "Solid immersion microscope," Appl. Phys. Lett. **57**, 2615–2616 (1990).
[7]J. B. Pendry, "Negative refraction makes a perfect lens," Phys. Rev. Lett. **85**, 3966–3969 (2000).
[8]X. Zhang and Z. Liu, "Superlenses to overcome the diffraction limit," Nat. Mater. **7**, 435–441 (2008).
[9]Z. Wang, W. Guo, L. Li, B. Luk'yanchuk, A. Khan, Z. Liu, Z. Chen, and M. Hong, "Optical virtual imaging at 50 nm lateral resolution with a white-light nanoscope," Nat. Commun. **2**, 218 (2011).
[10]A. Darafsheh, G. F. Walsh, L. Dal Negro, and V. N. Astratov, "Optical super-resolution by high-index liquid-immersed microspheres," Appl. Phys. Lett. **101**, 141128 (2012).
[11]R. Boudoukha, S. Perrin, A. Demagh, P. Montgomery, N.-E. Demagh, and S. Lecler, "Near- to far-field coupling of evanescent waves by glass microspheres," Photonics **8**, 73 (2021).
[12]A. V. Maslov and V. N. Astratov, "Optical nanoscopy with contact Mie-particles: Resolution analysis," Appl. Phys. Lett. **110**, 261107 (2017).
[13]S. Zhou, Y. Deng, W. Zhou, M. Yu, H. P. Urbach, and Y. Wu, "Effects of whispering gallery mode in microsphere super-resolution imaging," Appl. Phys. B: Lasers Opt. **123**, 236 (2017).
[14]A. Maslov and V. Astratov, "Resolution and reciprocity in microspherical nanoscopy: Point-spread function versus photonic nanojets," Phys. Rev. Appl. **11**, 064004 (2019).
[15]A. V. Maslov and V. N. Astratov, "Imaging of sub-wavelength structures radiating coherently near microspheres," Appl. Phys. Lett. **108**, 051104 (2016).
[16]X. Hao, C. Kuang, X. Liu, H. Zhang, and Y. Li, "Microsphere based microscope with optical super-resolution capability," Appl. Phys. Lett. **99**, 203102 (2011).
[17]S. Lecler, S. Perrin, A. Leong-Hoi, and P. Montgomery, "Photonic jet lens," Sci. Rep. **9**, 4725 (2019).
[18]A. Darafsheh, N. I. Limberopoulos, J. S. Derov, D. E. Walker, and V. N. Astratov, "Advantages of microsphere-assisted super-resolution imaging technique over solid immersion lens and confocal microscopies," Appl. Phys. Lett. **104**, 061117 (2014).
[19]L. Li, W. Guo, Y. Yan, S. Lee, and T. Wang, "Label-free super-resolution imaging of adenoviruses by submerged microsphere optical nanoscopy," Light: Sci. Appl. **2**, e104 (2013).
[20]H. Yang, N. Moullan, J. Auwerx, and M. A. Gijs, "Super-resolution biological microscopy using virtual imaging by a microsphere nanoscope," Small **10**, 1712–1718 (2014).
[21]A. Brettin, F. Abolmaali, K. F. Blanchette, C. L. McGinnis, Y. E. Nesmelov, N. I. Limberopoulos, D. E. Walker, I. Anisimov, A. M. Urbas, L. Poffo, A. V. Maslov, and V. N. Astratov, "Enhancement of resolution in microspherical nanoscopy by coupling of fluorescent objects to plasmonic metasurfaces," Appl. Phys. Lett. **114**, 131101 (2019).
[22]S. Perrin, H. Li, K. Badu, T. Comparon, G. Quaranta, N. Messaddeq, N. Lemercier, P. Montgomery, J.-L. Vonesch, and S. Lecler, "Transmission microsphere-assisted dark-field microscopy," Phys. Status Solidi (RRL) **13**, 1800445 (2019).
[23]S. Perrin, Y. J. Donie, P. Montgomery, G. Gomard, and S. Lecler, "Compensated microsphere-assisted interference microscopy," Phys. Rev. Appl. **13**, 014068 (2020).
[24]S. Perrin, H. Li, S. Lecler, and P. Montgomery, "Unconventional magnification behaviour in microsphere-assisted microscopy," Opt. Laser Technol. **114**, 40–43 (2019).
[25]H. S. S. Lai, F. Wang, Y. Li, B. Jia, L. Liu, and W. J. Li, "Super-resolution real imaging in microsphere-assisted microscopy," PLos One **11**, e0165194 (2016).
[26]H. Luo, H. Yu, Y. Wen, T. Zhang, P. Li, F. Wang, and L. Liu, "Enhanced high-quality super-resolution imaging in air using microsphere lens groups," Opt. Lett. **45**, 2981–2984 (2020).
[27]J. Zhou, B. Zeng, S. Bi, and Y. Wang, "Enhanced magnification factors in super-resolution imaging using stacked dual microspheres," J. Opt. **22**, 085605 (2020).
[28]G. Wu and M. Hong, "Optical nano-imaging via microsphere compound lenses working in non-contact mode," Opt. Express **29**, 23073–23082 (2021).
[29]J. Li, W. Liu, T. Li, I. Rozen, J. Zhao, B. Bahari, B. Kante, and J. Wang, "Swimming microrobot optical nanoscopy," Nano Lett. **16**, 6604–6609 (2016).
[30]B. Yan, Z. Wang, A. L. Parker, Y. Kun Lai, P. J. Thomas, L. Yue, and J. N. Monks, "Superlensing microscope objective lens," Appl. Opt. **56**, 3142–3147 (2017).
[31]G. Huszka and M. A. M. Gijs, "Turning a normal microscope into a super-resolution instrument using a scanning microlens array," Sci. Rep. **8**, 601 (2018).
[32]I. Kassamakov, S. Lecler, A. Nolvi, E. H. A. Leong-Hoi, and P. Montgomery, "3D super-resolution optical profiling using microsphere enhanced Mirau interferometry," Sci. Rep. **7**, 3683 (2017).

Downloaded from http://pubs.aip.org/aip/apl/article-pdf/doi/10.1063/5.0135346/16951738/161108_1_5.0135346.pdf

Published under an exclusive license by AIP Publishing

[33]P. Gerard, P. Benech, D. Khalil, R. Rimet, and S. Tedjini, "Towards a full vectorial and modal technique for the analysis of integrated optics structures: The radiation spectrum method (RSM)," Opt. Commun. **140**, 128–145 (1997).
[34]B. D. Guenther, *Modern Optics*, 2nd ed. (Oxford University Press, 2018).
[35]D. MjgEoasa, V. Viri, and M. Gijs, "Integration of highly-refractive spheres in microfluidic chips for high-contrast detection of bacteria with low-magnification systems," in SPIE Proceedings in Clinical and Preclinical Optical Diagnostics II (2019), paper No. 11076_56.
[36]Q. Lin, D. Wang, Y. Wang, L. Rong, J. Zhao, S. Guo, and M. Wang, "Super-resolution imaging by microsphere-assisted optical microscopy," Opt. Quantum Electron. **48**, 557 (2016).
[37]S. Bargiel, M. Baranski, M. Wiemer, J. Frömel, W.-S. Wang, and C. Gorecki, "Technological platform for vertical multi-wafer integration of microscanners and micro-optical components," Micromachines **10**, 185 (2019).
[38]J. C. Valencia-Estrada, R. B. Flores-Hernández, and D. Malacara-Hernández, "Singlet lenses free of all orders of spherical aberration," Proc. R. Soc. A: Math., Phys. Eng. Sci. **471**, 20140608 (2015).

Downloaded from http://pubs.aip.org/aip/apl/article-pdf/doi/10.1063/5.0135346/16951738/161108_1_5.0135346.pdf

Published under an exclusive license by AIP Publishing